



Studies of the nobility of phases using scanning Kelvin probe microscopy and its relationship to corrosion behaviour of Ni–Al bronze in chloride media



Q.N. Song^a, Y.G. Zheng^{a,*}, D.R. Ni^b, Z.Y. Ma^b

^a Key Laboratory of Nuclear Materials and Safety Assessment, Institute of Metal Research, Chinese Academy of Sciences, 62 Wencui Road, Shenyang 110016, China

^b Shenyang National Laboratory for Materials Science, Institute of Metal Research, Chinese Academy of Sciences, 72 Wenhua Road, Shenyang 110016, China

ARTICLE INFO

Article history:

Received 3 July 2014

Accepted 25 November 2014

Available online 2 December 2014

Keywords:

A. Copper

B. EPMA

B. AFM

C. Acid corrosion

C. Welding

ABSTRACT

An as-cast Ni–Al bronze (NAB) was subjected to friction-stir processing. The microstructure, nobility of the phases and corrosion behaviour of the as-cast and friction-stir processed NAB were studied using EPMA, scanning Kelvin probe force microscopy (SKPFM) and SEM, respectively. SKPFM results revealed that the κ phase in the as-cast NAB and the small-sized phases inside β' in the friction-stir processed NAB exhibited relatively lower nobility. These phases were preferentially corroded in acidic chloride solution but protected in neutral chloride solution. The correlation between the nobility of the phases and the practical corrosion behaviour was also discussed.

© 2014 Elsevier Ltd. All rights reserved.

1. Introduction

Ni–Al bronze (NAB) is a common material used for ship propellers because of its high strength, fracture toughness and corrosion/cavitation erosion resistance in seawater environments [1–3]. NAB is a quaternary alloy with Cu as the main element, and contains 9–12 wt.% Al and 6 wt.% each of Fe and Ni. NAB undergoes complex phase transformation during the casting process. An as-cast NAB is mainly composed of Widmanstätten α phase, several intermetallics, i.e., κ phases with abundant Al, Fe or Ni and some β' (retained high-temperature β) phases [4,5]. According to Weill-Couly and Arnaud [6], κ phases are categorized into four types according to their morphologies. κ_I is globular or rosette shaped and is based on Fe_3Al . κ_{II} exhibits similar morphology and composition, but it is smaller in size than κ_I . κ_{III} is lamellar and is based on NiAl. κ_{IV} precipitates inside the α phase and is abundant in Fe. The performance of these phases varies in different chloride media [1,3,7,8]. In seawater environments, β' and the lamellar α phase adjacent to κ_{III} were preferentially corroded, whereas no sign of attack was found at κ_I and κ_{II} [1,3]. In crevice corrosion environments with low pH and highly concentrated chloride ions, κ_{III} was anodic with regard to the lamellar α [7]. Moreover, NAB exhibited pH-dependent behaviour in aqueous chloride media. The Cu-abundant α

phase was corroded at pH higher than 4.0, whereas the Fe-, Ni- and Al-abundant κ_I , κ_{II} and κ_{IV} were corroded at pH lower than 4.0 [8].

Friction-stir processing (FSP) is a novel solid-state method that originates from friction-stir welding [9]. During FSP, a non-consumable rotating tool inserts into a component and then traverses along the preferred path to modify the microstructure [10]. FSP has been applied to Ti-, Al-, Cu-based alloys, etc. [11–17]. FSP modified the microstructure and improved the mechanical properties and corrosion/cavitation erosion resistance of the as-cast NAB [13–17]. However the corrosion behaviour of the friction-stir processed NAB (noted as FSPed NAB hereinafter) in different chloride media has not been investigated.

Scanning Kelvin probe force microscopy (SKPFM) combines the Kelvin probe techniques with atomic force microscopy (AFM); this method enables the concurrent mapping of topography and Volta potential distribution of the metal surface in vacuum or air. It was reported that the Volta potentials of metals covered with ultrathin electrolyte layers obtained using a standard Kelvin probe were linearly correlated with the corrosion potentials measured in the electrolyte layers [18,19]. Schmutz et al. [20] also reported that the Volta potentials measured in air through SKPFM for pure metals were linearly related to the open-circuit potentials measured in aqueous solutions. Moreover, the Volta potential map demonstrated the relative nobility and possible corrosion tendency of each phase in the metal [21]. SKPFM has been used to characterise

* Corresponding author. Tel.: +86 24 23928381; fax: +86 24 23894149.

E-mail address: ygzheng@imr.ac.cn (Y.G. Zheng).

the nobility of the phases of Al alloys, stainless steels, Mg alloys, etc. The correlation between the SKPFM results and the practical corrosion behaviour has also been discussed [21–25]. However, to our knowledge, the application of SKPFM in characterising the nobility of the phases of NAB has only been reported by Nakhaie et al. [26]. In their research, the Volta potential results showed that the κ phases exhibited lower nobility; correspondingly these phases were the preferential sites for corrosion initiation in 0.1 M HCl solution [26]. Moreover, the nobility of the phases of the FSPed NAB and its correlation with the practical corrosion behaviour have not been investigated.

In this study, the nobility of the phases of the as-cast and FSPed NAB was characterised through SKPFM. The corrosion behaviour in different chloride media was studied by conducting immersion tests. The correlation between the nobility of the phases and the practical corrosion behaviour was also discussed.

2. Experimental

2.1. Materials and characterisation

An as-cast UNS C95800 NAB (chemical composition in wt.%: Al, 9.18; Ni, 4.49; Fe, 4.06; Mn, 1.03 and Cu balance) with a dimension of 300 mm \times 70 mm \times 8 mm was subjected to FSP. A nickel-based alloy tool comprising a concave shoulder with a diameter of 24 mm, and a threaded conical pin with a root diameter of 8 mm and a length of 7 mm was used. The rotating rate and traverse speed of the processing tool were 1,200 rpm and 50 mm/min, respectively. The tilt angle of the tool was 3°. The tool and the processed plate were cooled with blowing air during FSP. The microstructures of the as-cast and FSPed NAB were observed with an optical microscope after etching with a solution containing 5 g of FeCl₃, 2 mL of HCl and 95 mL of C₂H₅OH. A minimum of 30 equivalent grains or particles were randomly selected to determine the general size of each phase in the microstructure. An electron probe micro-analyser (1610, Shimadzu) was used to characterise the element distribution in the microstructure.

2.2. SKPFM measurements

SKPFM measurements were conducted using a Multimode IIID Scanning Probe Microscope (SPM) system (Bruker Corporation, Santa Barbara, CA) to obtain the Volta potential maps of the as-cast and FSPed NAB. The samples for SKPFM measurements were mechanically and successively ground with abrasive papers up to 5000 grit, then they were mechanically polished using diamond paste to 0.5 μ m and polished again using colloidal silica suspension to 0.02 μ m to remove polishing scratches. SKPFM measurements were conducted in air at ambient temperature, pressure and humidity. For the as-cast and FSPed NAB, the measurements were repeated at least three times to ensure reproducibility. The tips used were magnetic etched silicon probes (MESP type, Bruker Corporation, CA, USA) with a length of 200–250 μ m and a resonant frequency of 60–100 kHz. A dual-scan mode was used. Tapping mode was used in the first scan to obtain the surface topography signal, and the tip was lifted up 50 nm in the second scan to obtain the Volta potential signal. In SKPFM measurements, an AC voltage was applied on the tip to induce a harmonic oscillation of the cantilever. A DC voltage was then added to balance the electric field between the tip and the sample and stop the oscillation. The added DC voltage was derived from the contact potential difference (CPD) between the tip and the sample; CPD was defined as $V_{CPD} = (\Phi_{tip} - \Phi_{sample})/e$, where Φ_{tip} and Φ_{sample} are the work functions of the

tip and the sample, respectively, and e is the value of the electronic charge [27]. The value of Φ_{tip} was constant in the present study; thus, higher V_{CPD} resulted in lower work function of the sample. The work function is defined as the minimum energy required for an electron to escape from the surface of a solid. The lower work function of a material caused an easy occurrence of corrosion [28]. V_{CPD} was directly measured through SKPFM and noted as the Volta potential in this study. Hence, the areas with higher potentials in the Volta potential maps were speculated to be more electrochemically active than those with lower potentials. The Volta potential difference between two different phases in the microstructure was referred to “VPD”.

2.3. Corrosion tests

Corrosion behaviour was investigated by conducting immersion tests in two different chloride media, i.e., aerated neutral and acidic (pH = 2) 3.5 wt.% NaCl solutions, at room temperature for the as-cast and FSPed NAB. Neutral 3.5 wt.% NaCl solution was prepared from analytical-grade reagent and distilled water, and pH was adjusted using HCl to produce the acidic 3.5 wt.% NaCl solution. The samples were ground successively with abrasive papers up to 5000 grit and mechanically polished using diamond paste to 0.5 μ m. The samples were observed with a scanning electron microscope (FEI-Inspect F) after immersion for a specific period of time.

3. Results

3.1. Microstructure

Fig. 1 shows the microstructures of the as-cast and FSPed NAB. The as-cast NAB is composed of higher than 100- μ m coarse Widmanstätten α phases, lamellar eutectoid $\alpha + \kappa_{III}$, κ_{II} , κ_{IV} and some β' phases, as shown in Fig. 1a. κ_{II} is mainly distributed at the phase boundaries with a size of 1–3 μ m, and κ_{IV} is precipitated inside the α phase with a size lower than 1 μ m. The stirred zone in the FSPed NAB contains four different microstructures along the plate thickness, namely Widmanstätten α and fine β' phases, banded α and β' , equiaxed α and β' and stream-like α and β' from the surface to the bottom; these microstructures were described in detail in our previous study [13]. Only the equiaxed microstructure was evaluated in this work because it possesses most of the stirred zone. As shown in Fig. 1b, the lightly etched α is about 10 μ m and the equiaxed α and β' phases are uniformly distributed in the FSPed NAB.

Fig. 2 shows the electron probe micro-analysis (EMPA) results of the as-cast and FSPed NAB. For the as-cast NAB, κ_{II} , the lamellar κ_{III} and α are in dark, grey and white contrasts, respectively, as shown in the back-scattered electron (BSE) image in Fig. 2a. Element distribution maps shown in Fig. 2b–d illustrate the following. κ_{II} contains the highest Al content, followed by κ_{III} and α . Fe is the most enriched in κ_{II} . Ni is abundant in κ_{II} and κ_{III} . The composition of a small feature is influenced by its surrounding phases. The element distribution of κ_{IV} inside α is not verified here because of its small size. Moreover, confirming the differences in element contents between the lamellar α and κ_{III} is difficult because they are very close to each other. For the FSPed NAB, the dark, grey and white areas in Fig. 2e correspond to the small-sized phase inside β' , β' and α , respectively. Fig. 2f–h show that the small-sized phase inside β' contains the highest Al and Fe contents, followed by β' . Ni is enriched in the small-sized phases and their surrounding β' . Evidently these alloying elements are more uniformly distributed in the FSPed NAB than in the as-cast NAB.

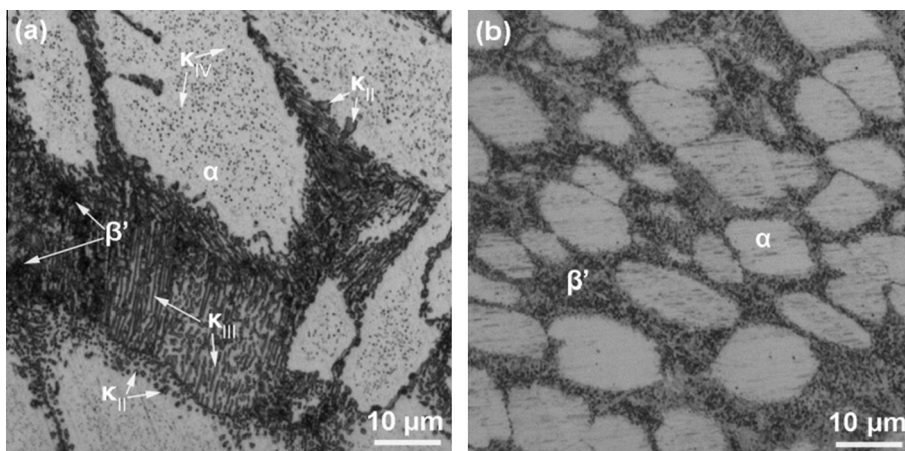


Fig. 1. Optical microstructures for the (a) as-cast and (b) FSPed NAB.

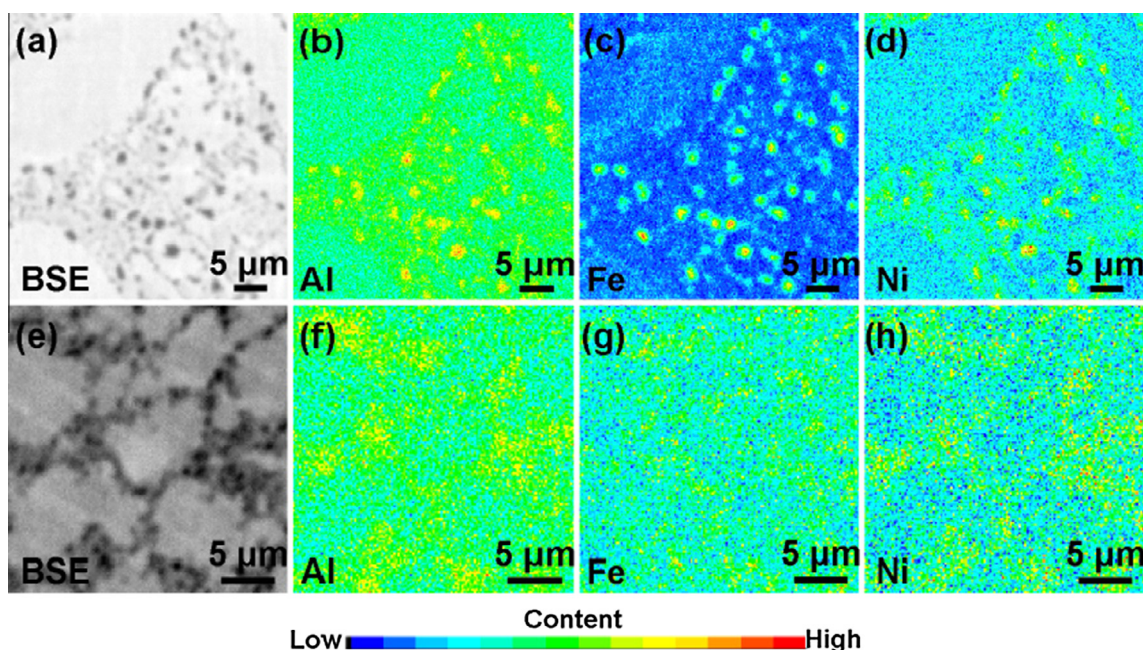


Fig. 2. EPMA results for the (a–d) as-cast and (e–h) FSPed NAB: (a, e) BSE images; (b, f) distribution of Al; (c, g) distribution of Fe; and (d, h) distribution of Ni.

3.2. Volta potential obtained through SKPFM

The topography images and Volta potential maps of the as-cast and FSPed NAB are shown in Fig. 3. The brighter areas in the Volta potential map correspond to the microstructures with higher Volta potentials and are less noble than the darker areas. For the as-cast NAB, κ_{II} and κ_{III} present higher Volta potentials than α , as shown in Fig. 3b. Moreover, small-sized phases with higher Volta potentials are distributed inside the α matrix and they correspond to the κ_{IV} phases. For the FSPed NAB, the small-sized phases inside β' exhibit higher potentials, as demonstrated in Fig. 3d. The Volta potentials are higher at locations where the small-sized phases are densely distributed, as presented in the white box in Fig. 3d. However, the Volta potentials are relatively lower at locations where these small-sized phases are sparsely distributed, as shown in the black box. Contamination, such as silica suspension (as indicated by the arrows), remains on the polished surface. The areas with contamination were excluded when analysing the Volta potentials.

The line scan profiles of the Volta potential maps are presented here to investigate the VPDs among different phases, as shown in

Figs. 4 and 5. For the as-cast NAB, the line scan profiles analysing the VPDs between α and κ_{II} , α and κ_{III} and α and κ_{IV} are shown in Fig. 4b, c and d, respectively. For the FSPed NAB, Fig. 5b and c demonstrate the line scan analysis at locations where the small-sized phases inside β' are densely and sparsely distributed, respectively. VPDs among the phases are listed in Table 1. A minimum of five lines were selected to determine each VPD range.

3.3. Corrosion behaviour in acidic 3.5 wt.% NaCl solution

Figs. 6 and 7 show the surface morphologies of the as-cast and FSPed NAB, respectively, after immersion in acidic 3.5 wt.% NaCl solution for different periods. For the as-cast NAB, κ_{II} and κ_{IV} are dissolved after immersion for 20 min as presented in Fig. 6a and b. The lamellar κ_{III} are not corroded. After immersion for 6 h, almost all the κ_{II} phases are dissolved, leaving larger pits (Fig. 6c). The lamellar κ_{III} is also dissolved, as demonstrated in Fig. 6d. For the FSPed NAB, the small-sized phases inside β' are dissolved after immersion for 20 min, as shown in Fig. 7a and b, whereas β' is corroded after immersion for 6 h (Fig. 7c and d).

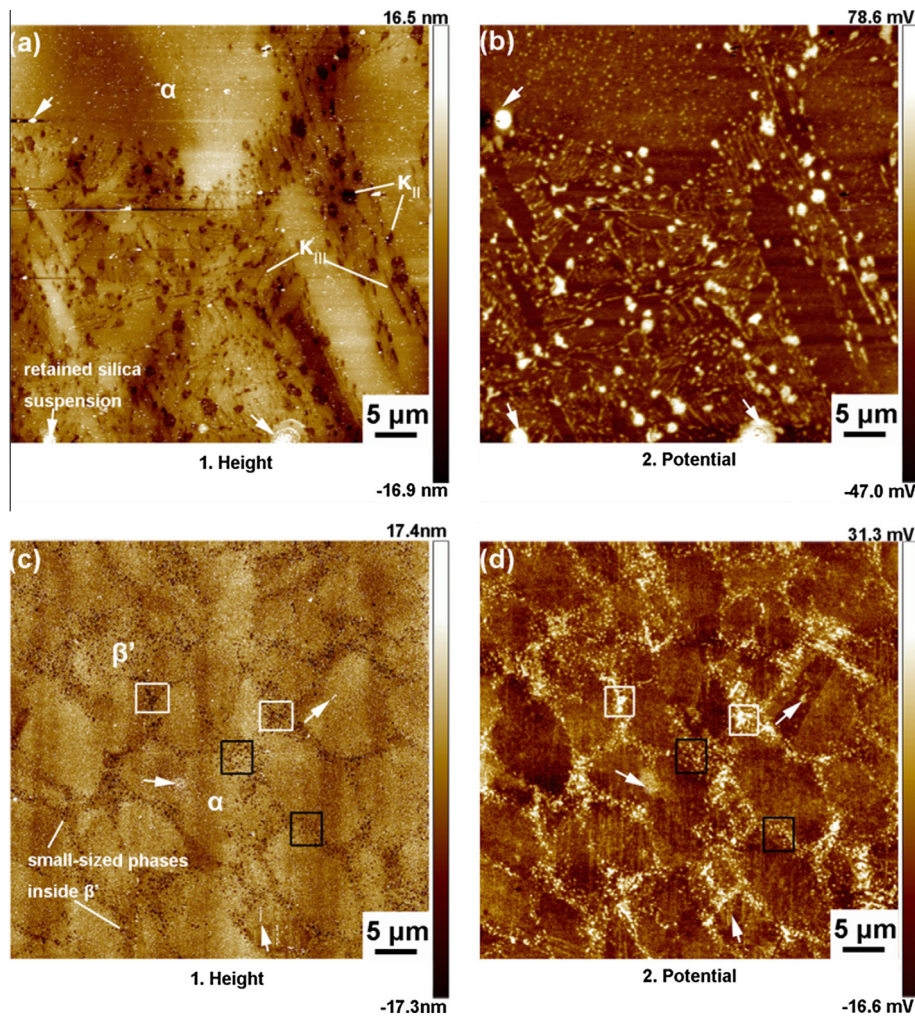


Fig. 3. (a, c) Topography images and (b, d) Volta potential maps for the as-cast and FSPed NAB: (a, b) for the as-cast NAB and (c, d) for the FSPed NAB.

The as-cast NAB suffers more severe attack in acidic 3.5 wt.% NaCl solution.

3.4. Corrosion behaviour in neutral 3.5 wt.% NaCl solution

Fig. 8a and b present the surface morphologies of the as-cast and FSPed NAB after immersion in neutral 3.5 wt.% NaCl solution for 6 h. For the as-cast NAB, κ_{II} and the lamellar κ_{III} are not dissolved, whereas the α matrix adjacent to κ_{II} and the lamellar α are preferentially corroded as shown in Fig. 8a. For the FSPed NAB, β' suffers from preferential corrosion, α is protected and the small-sized phases inside β' are retained as indicated in Fig. 8b. The κ phases of the as-cast NAB and the small-sized phases inside β' of the FSPed NAB are still retained after long-term immersion in neutral 3.5 wt.% NaCl solution as demonstrated in Fig. 8c and d, respectively. The insert image in Fig. 8c shows that κ_{IV} is retained and its surrounding α matrix is dissolved.

4. Discussion

4.1. Volta potential analysis

The Volta potential measurements through SKPFM were used to characterise the nobility of different phases of the as-cast and FSPed NAB. The measured Volta potential was related to the chem-

ical composition for a specific feature [29]. For the as-cast NAB, Fe or Al was more enriched in κ_{II} and κ_{III} as indicated by the EPMA results as shown in Fig. 2b and c. Considering that the work function of Cu is higher than that of Fe and Al [30], κ_{II} and κ_{III} possessed lower work functions and correspondingly exhibited higher Volta potentials than the Cu-rich α . κ_{II} exhibited the highest Volta potential because it contained the highest Fe and Al contents; hence κ_{II} presented the lowest nobility. Nakhaie et al. [26] also reported that the κ phases exhibited lower nobility than α , and κ_I with the highest Fe and Al contents demonstrated the lowest nobility. κ_{II} and κ_{IV} were both based on Fe_3Al [31]; therefore, the Volta potential of κ_{IV} was also higher than that of α . However, κ_{IV} exhibited lower Volta potential than κ_{II} in the present study. This finding could be explained as follows. The Volta potential of a small-surface feature measured through SKPFM includes the contribution from the surrounding matrix; it is the average value of the potentials of the feature and the surrounding region [32]. It was reported that the VPD between the chromium nitride and its surrounding matrix was lower when the nitride was smaller in size in isothermally aged duplex stainless steels [32]. Hence, as a result of the contribution from the surrounding α matrix, κ_{IV} exhibited lower Volta potential even if its composition was similar to that of κ_{II} . The lamellar NiAl-based κ_{III} demonstrated lower Volta potential than the Fe_3Al -based κ_{II} because the former contained higher Ni content [5] and the work function of Ni is higher than that of Al and Fe [30]. This finding was also consistent with the results shown in the study of Nak-

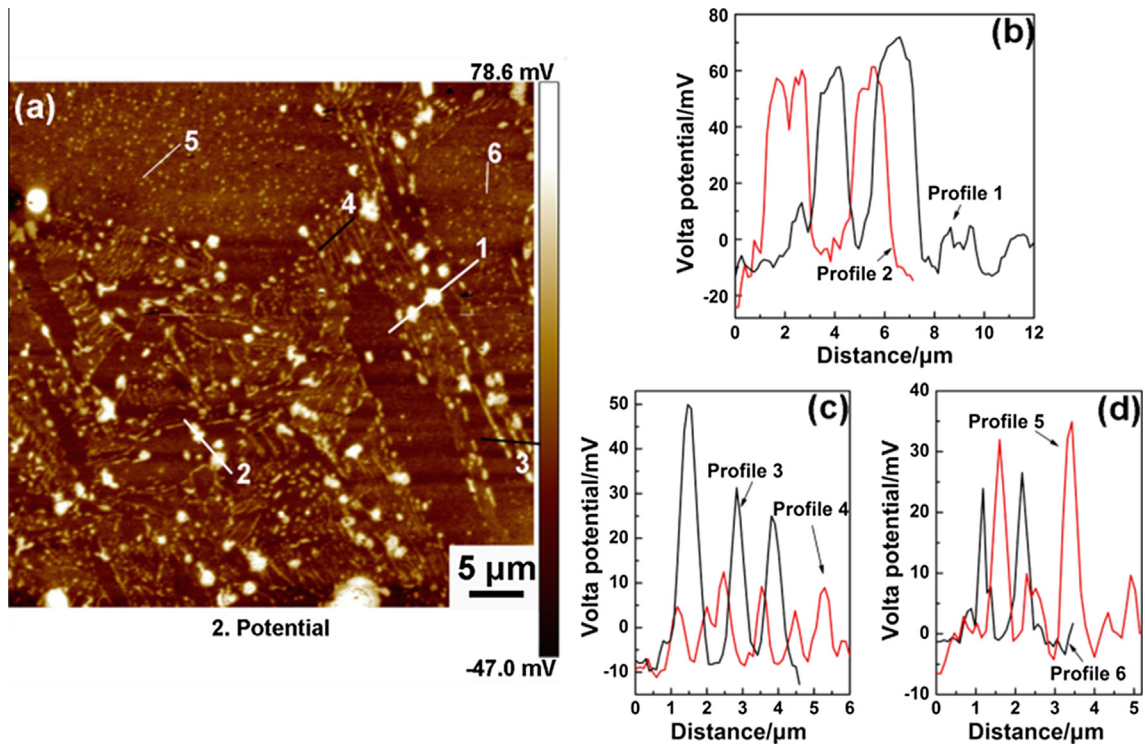


Fig. 4. (a) Volta potential map and line scan profiles for (b) α/κ_{II} , (c) α/κ_{III} and (d) α/κ_{IV} of the as-cast NAB.

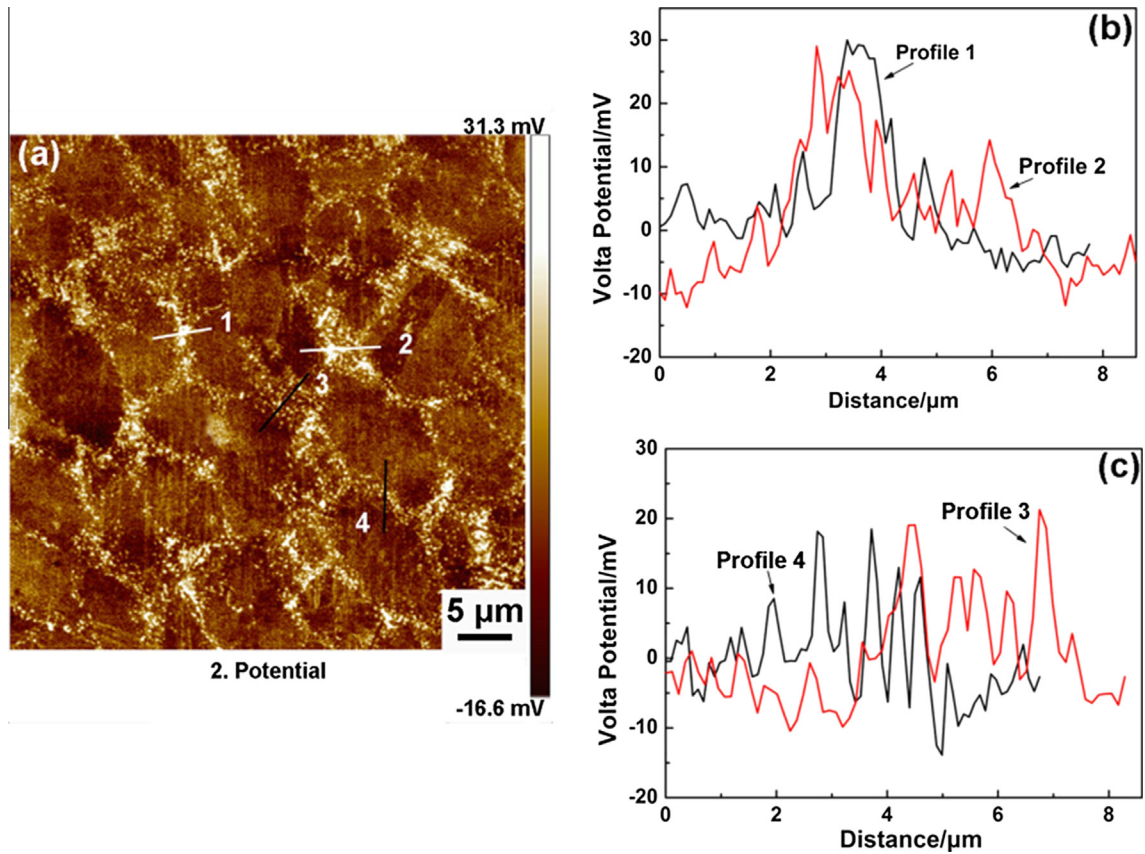


Fig. 5. (a) Volta potential map and line scan profiles for (b) α /densely distributed small-sized phases inside β' and (c) α /sparsely distributed small-sized phases inside β' of the FSPed NAB.

Table 1
VPDs among the phases of the as-cast and FSPed NAB.

Phases	As-cast NAB			FSPed NAB	
	α/κ_{II}	α/κ_{III}	α/κ_{IV}	α/β'	$\alpha/\text{small-sized phases inside } \beta'$
VPD (mV)	60–80	10–30 (up to 60)	20–40	Hardly distinguished	15–35

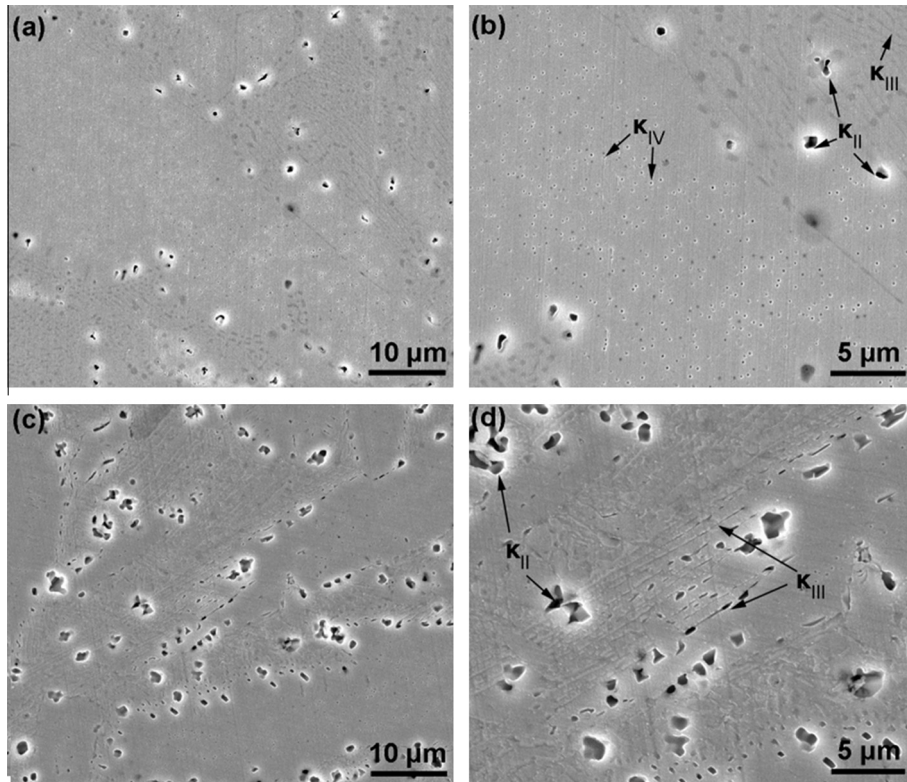


Fig. 6. Surface morphologies of the as-cast NAB after immersion in acidic 3.5 wt.% NaCl solution (pH = 2) for (a, b) 20 min and (c, d) 6 h: (a, c) in small magnification; and (b, d) in large magnification.

haie et al. [26]. In the present study, the Volta potentials of the κ_{III} phases were higher at some locations (line 4 in Fig. 4c) because these κ_{III} phases were in wider lamellar structure than those at line 3 in Fig. 4c, consequently the contribution from the surrounding phases to the measured Volta potential became smaller.

For the FSPed NAB, the small-sized phases inside β' presented the highest Volta potential because they contained the highest Al and Fe contents, as indicated in Fig. 2f and g. They were considered to be the retained κ_{II} phases from the cast microstructure. The κ_{II} phases in the cast microstructure would be dissolved and transformed to the high temperature β when the temperature exceeded 930 °C [31]. Our previous study showed that the highest temperature was lower than 930 °C in the centre of the stirred zone of the FSPed NAB [13]. Therefore, κ_{II} probably underwent recrystallization and was refined because of the severe stirring during FSP. However, in the present study, the VPD between α and the small-sized phase inside β' in the FSPed NAB (15–35 mV) was relatively lower than that between α and κ_{II} (60–80 mV) in the as-cast NAB. This finding could be explained as follows. At temperature higher than 860 °C, the κ_{IV} phases in the cast microstructure would be dissolved [31]. In this study, the κ_{IV} phases were dissolved into α during FSP and not precipitated during the fast cooling process, as indicated in the microstructure of the FSPed NAB (Figs. 1b and 2e), which lacked κ_{IV} . Consequently the Al and Fe contents increased in α . The difference in Al and Fe contents between

α and the small-sized phase inside β' was reduced, resulting in lower VPD. Moreover, the small-size phase inside β' was much smaller than κ_{II} . The measured Volta potential of the small-sized phase was influenced by the surrounding β' and was consequently lower than that of κ_{II} . This also resulted in lower VPD between α and the small-sized phase inside β' in the FSPed NAB.

The small-sized phases inside β' which were densely distributed exhibited higher Volta potentials than those that were sparsely distributed, as shown in Fig. 3d. For the sparsely distributed regions, an evident contribution from the surrounding β' was included in the measured Volta potential of the small-sized phase. However, for the densely distributed regions, the contribution from the surrounding β' was significantly reduced and these small-sized phases were equal to a large-sized phase. Therefore, verifying the Volta potential of a single small-sized phase in the white box in Fig. 3d was difficult even if these phases were separated as shown in Fig. 3c. When the temperature exceeded 800 °C during FSP, the lamellar eutectoid, i.e., $\alpha + \text{NiAl}$ -based κ_{III} in the cast microstructure would be transformed into the high-temperature β [31]. β' was formed during subsequent rapid cooling process. Therefore, β' contained more Al and Ni than α , as indicated by the EPMA results in Fig. 2f and h. However, the VPD between α and β' could not be verified because α and β' were both Cu-rich phases [5], the small difference in the contents of the alloying elements, i.e., Fe, Al and Ni, would not result in evident VPD.

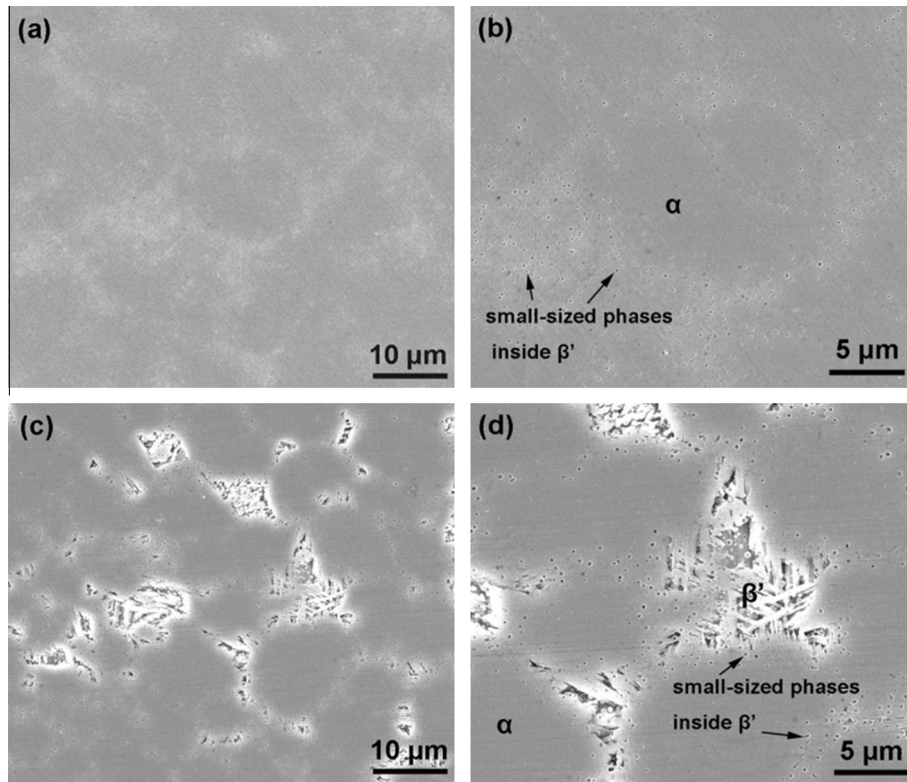


Fig. 7. Surface morphologies of the FSPed NAB after immersion in acidic 3.5 wt.% NaCl solution (pH = 2) for (a, b) 20 min and (c, d) 6 h: (a, c) in small magnification; and (b, d) in large magnification.

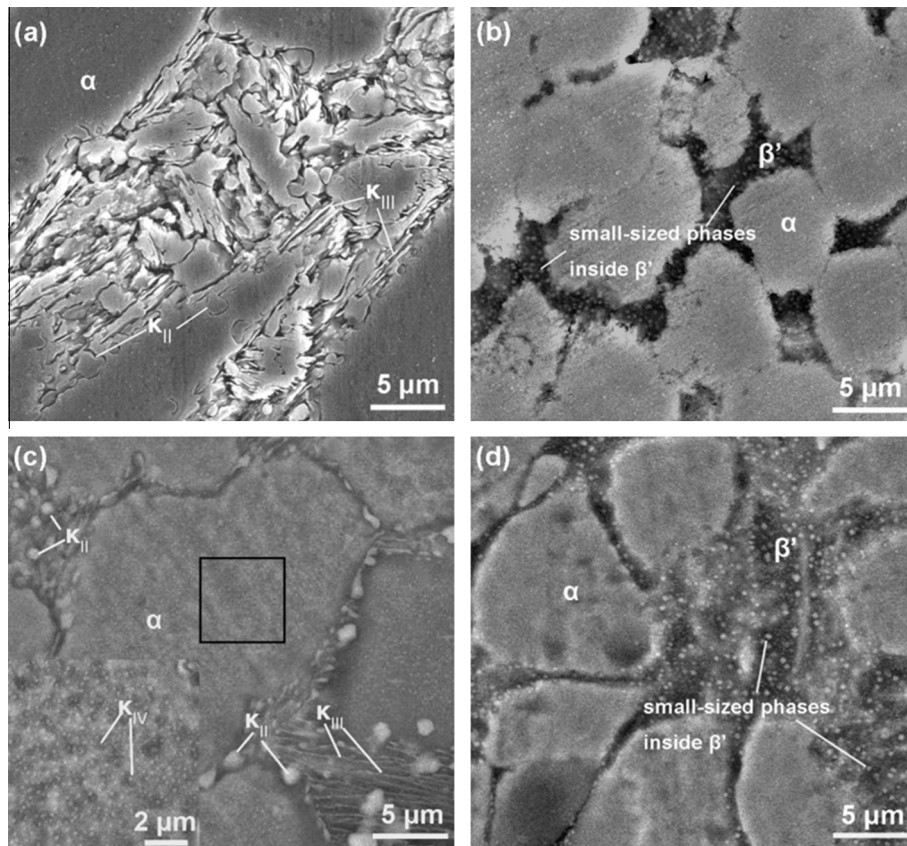


Fig. 8. Surface morphologies of the as-cast and FSPed NAB after immersion in neutral 3.5 wt.% NaCl solution. As-cast NAB: (a) 6 h, (c) 15 d; FSPed NAB: (b) 6 h, (d) 15 d.

4.2. Relationship between the nobility of phases and corrosion behaviour

As shown in Fig. 6, the κ phases in the as-cast NAB were preferentially corroded in acidic 3.5 wt.% NaCl solution. This result was in agreement with the SKPFM result shown in Fig. 4, which indicated that the κ phases with higher Volta potential exhibited lower nobility. κ_{II} was first corroded because it exhibited the highest Volta potential, i.e., the lowest nobility. As discussed in the previous section, κ_{IV} possessed similar composition to κ_{II} and thus it was also corroded. κ_{III} demonstrated a relatively lower Volta potential, i.e., higher nobility; hence it became corroded after the corrosion of κ_{II} and κ_{IV} . As shown in Fig. 7, the small-sized phases inside β' in the FSPed NAB suffered preferential corrosion because they exhibited the highest Volta potential, as demonstrated in Fig. 5. β' became corroded with the increasing immersion time, indicating that it possessed lower nobility than α ; however, this finding was not verified through SKPFM.

Guo et al. [33] studied the corrosion behaviour of duplex stainless steel 2507 at different annealing temperatures and found that higher VPD between the ferrite and austenite generated higher driving force of corrosion, and thus resulted in higher corrosion rate. In the present study, FSP homogenised and refined the cast microstructure. Correspondingly, the VPDs among the phases in the FSPed NAB were lower than those in the as-cast NAB. Therefore, the FSPed NAB was less severely attacked in acidic 3.5 wt.% NaCl solution than the as-cast NAB, as shown in Figs. 6 and 7.

In neutral 3.5 wt.% NaCl solution, the κ phases in the as-cast NAB exhibited cathodic behaviour with regard to α , as shown in Fig. 8a and c. This finding was contrary with the nobility results obtained through SKPFM. According to Wharton et al. [34], Al exhibited higher affinity for oxygen than Cu and Al_2O_3 was more stable than Cu_2O . The Al-abundant κ phases were protected in approximately neutral chloride media because a protective Al_2O_3 film was formed on them [7]. However, the aluminium oxide/hydroxide film was unstable with the pH of the corrosive media lower than 4. In acidic chloride media, the protection for the κ phases caused by the protective Al_2O_3 film was lost, and the κ phases became anodic with regard to the Cu-abundant α [7]. Hence, the VPD results obtained through SKPFM should be carefully interpreted when evaluating the corrosion behaviour of the materials because the alloying element would be in different states, i.e., active or passive in different corrosive media.

Analogously, the small-sized phases inside β' in the FSPed NAB that contained the highest Al content were protected because of the formation of a protective Al_2O_3 film in neutral 3.5 wt.% NaCl solution, as shown in Fig. 8b and d. β' contained higher Al content than α but was preferentially corroded, probably due to its direct contact with the cathodic sites, i.e., the small-sized phases. Moreover, the martensitic structure of β' might also contribute to its preferential corrosion. It was reported that the retained β in the as-cast NAB and the martensitic β phase in the metal inert-gas-welded NAB (i.e., β') were preferentially corroded in seawater [6,35]. In acidic 3.5 wt.% NaCl solution, protection for the small-sized phases inside β' was lost with the absence of the protective Al_2O_3 film and the small-sized phases were preferentially corroded.

5. Conclusions

In this research, an as-cast NAB was subjected to FSP. The nobility of the phases of the as-cast and FSPed NAB was characterised through SKPFM, and its correlation with the practical corrosion behaviour was also explored. The main findings were presented as follows:

- (1) In the as-cast NAB, κ_{II} exhibited the highest Volta potential, i.e., lowest nobility, because it contained the highest Al and Fe contents, followed by κ_{IV} , κ_{III} and α . In the FSPed NAB, the small-sized phase inside β' exhibited the lowest nobility because of its highest Al content, followed by β' and α .
- (2) In acidic 3.5 wt.% NaCl solution, the κ phases in the as-cast NAB and the small-sized phases inside β' in the FSPed NAB were preferentially dissolved because of their low nobilities. The FSPed NAB suffered less severe attack than the as-cast NAB because FSP reduced the VPDs among the phases of the as-cast NAB.
- (3) The κ phases in the as-cast NAB and the small-sized phases inside β' in the FSPed NAB were protected in neutral 3.5 wt.% NaCl solution. This finding was probably due to the formation of a protective Al_2O_3 film.
- (4) The SKPFM results should be carefully interpreted when evaluating the corrosion behaviour because the alloying element exhibited different performance, i.e., being activated or passivated in different corrosive media.

Acknowledgements

This work was supported by the National Natural Science Foundation of China (No. 51131008). The authors also acknowledge the suggestions given by Dr. S.Y. Wang on conducting and analysing the experiments.

References

- [1] E.A. Culpan, G. Rose, Corrosion behavior of cast nickel aluminum bronze in seawater, *Br. Corros. J.* 14 (1979) 160–166.
- [2] A.H. Tuthill, Guidelines for the use of copper alloys in seawater, *Mater. Perform.* 26 (1987) 12–22.
- [3] A. Al-Hashem, P.G. Caceres, W.T. Riad, H.M. Shalaby, Cavitation corrosion behavior of cast nickel–aluminum bronze in seawater, *Corrosion* 51 (1995) 331–342.
- [4] E.A. Culpan, G. Rose, Microstructural characterization of cast nickel aluminium bronze, *J. Mater. Sci.* 13 (1978) 1647–1657.
- [5] A. Jahanafrooz, F. Hasan, G.W. Lorimer, N. Ridley, Microstructural development in complex nickel–aluminium bronzes, *Metall. Trans. A* 14A (1983) 1951–1956.
- [6] P. Weill-Couly, D. Arnaud, Effect of composition and structure of Al bronzes on their behaviour in service, *Fonderie* 28 (1973) 123–135.
- [7] J.A. Wharton, K.R. Stokes, The influence of nickel–aluminum bronze microstructure and crevice solution on the initiation of crevice corrosion, *Electrochim. Acta* 53 (2008) 2463–2473.
- [8] S. Neodo, D. Carugo, J.A. Wharton, K.R. Stokes, Electrochemical behavior of nickel–aluminum bronze in chloride media: Influence of pH and benzotriazole, *J. Electroanal. Chem.* 695 (2013) 38–46.
- [9] W.M. Thomas, E.D. Nicholas, J.C. Needham, M.G. Murch, P. Temple-Smith, C.J. Dawes, G.B. Patent Application No. 9125978.8, 1991.
- [10] R.S. Mishra, Z.Y. Ma, Friction-stir welding and processing, *Mater. Sci. Eng. R* 50 (2005) 1–78.
- [11] M. Atapour, A. Pilchak, G.S. Frankel, J.C. Williams, Corrosion behaviour of investment cast and friction stir processed Ti–6Al–4V, *Corros. Sci.* 52 (2010) 3062–3069.
- [12] M.L. Santella, T. Engstrom, D. Storzjohann, T.-Y. Pan, Effects of friction stir processing on mechanical properties of the cast aluminum alloys A319 and A356, *Scripta Mater.* 53 (2005) 201–206.
- [13] D.R. Ni, P. Xue, D. Wang, B.L. Xiao, Z.Y. Ma, Inhomogeneous microstructure and mechanical properties of friction stir processed NiAl bronze, *Mater. Sci. Eng. A* 524 (2009) 119–128.
- [14] D.R. Ni, B.L. Xiao, Z.Y. Ma, Y.X. Qiao, Y.G. Zheng, Corrosion properties of friction-stir processed cast NiAl bronze, *Corros. Sci.* 52 (2010) 1610–1617.
- [15] K. Oh-Ishi, T.R. McNelley, Microstructural modification of as-cast NiAl bronze by friction-stir processing, *Metall. Mater. Trans. A* 35A (2004) 2951–2961.
- [16] Q.N. Song, Y.G. Zheng, S.L. Jiang, D.R. Ni, Z.Y. Ma, Comparison of corrosion and cavitation erosion behaviors between the as-cast and friction-stir processed nickel aluminum bronze, *Corrosion* 69 (2013) 1111–1121.
- [17] Q.N. Song, Y.G. Zheng, D.R. Ni, Z.Y. Ma, Corrosion and cavitation erosion behaviors of friction stir processed Ni–Al bronze: effect of processing parameters and position in the stirred zone, *Corrosion* 70 (2014) 261–270.
- [18] M. Stratmann, The investigation of the corrosion properties of metals, covered with adsorbed electrolyte layers – a new experimental technique, *Corros. Sci.* 27 (1987) 869–872.

- [19] M. Stratmann, H. Streckel, On the atmospheric corrosion of metals which are covered with thin electrolyte layers – I. Verification of the experimental technique, *Corros. Sci.* 30 (1990) 681–696.
- [20] P. Schmutz, G.S. Frankel, Characterization of AA2024–T3 by scanning Kelvin probe force microscopy, *J. Electrochem. Soc.* 145 (1998) 2285–2295.
- [21] A. Davoodi, J. Pan, C. Leygraf, S. Norgren, The role of intermetallic particles in localized corrosion of an aluminum alloy studied by SKPFM and integrated AFM/SECM, *J. Electrochem. Soc.* 155 (2008) C211–C218.
- [22] J.H.W. de Wit, Local potential measurements with the SKPFM on aluminium alloys, *Electrochim. Acta* 49 (2004) 2841–2850.
- [23] M. Sababi, S. Ejnermark, J. Andersson, P.M. Claesson, J. Pan, Microstructure influence on corrosion behavior of a Fe–Cr–V–N tool alloy studied by SEM/EDS, scanning Kelvin force microscopy and electrochemical measurement, *Corros. Sci.* 66 (2013) 153–159.
- [24] N. Sathirachinda, R. Pettersson, J. Pan, Depletion effects at phase boundaries in 2205 duplex stainless steel characterized with SKPFM and TEM/EDS, *Corros. Sci.* 51 (2009) 1850–1860.
- [25] M. Jönsson, D. Thierry, N. LeBozec, The influence of microstructure on the corrosion behaviour of AZ91D studied by scanning Kelvin probe force microscopy and scanning Kelvin probe, *Corros. Sci.* 48 (2006) 1193–1208.
- [26] D. Nakhaie, A. Davoodi, A. Imani, The role of constituent phases on corrosion initiation of NiAl bronze in acidic media studied by SEM–EDS, AFM and SKPFM, *Corros. Sci.* 80 (2013) 104–110.
- [27] M. Li, L.Q. Guo, L.J. Qiao, Y. Bai, The mechanism of hydrogen-induced pitting corrosion in duplex stainless steel studied by SKPFM, *Corros. Sci.* 60 (2012) 76–81.
- [28] W. Li, D.Y. Li, Variations of work function and corrosion behaviors of deformed copper surfaces, *Appl. Surf. Sci.* 240 (2005) 388–395.
- [29] O.A. Semenikhin, L. Jiang, T. Iyoda, K. Hashimoto, A. Fujishima, A Kelvin probe force microscopic study of the local dopant distribution in conducting polybithiophene, *Electrochim. Acta* 42 (1997) 3321–3326.
- [30] H. Stanislaw, D. Tomasz, Work functions of elements expressed in terms of the Fermi energy and the density of free electrons, *J. Phys. Condens. Matter* 10 (1998) 10815–10826.
- [31] K. Oh–ishi, T.R. McNelley, The influence of friction stir processing parameters on microstructure of as-cast NiAl bronze, *Metall. Mater. Trans. A* 36A (2005) 1575–1585.
- [32] N. Sathirachinda, R. Pettersson, S. Wessman, J. Pan, Study of nobility of chromium nitrides in isothermally aged duplex stainless steels by using SKPFM and SEM/EDS, *Corros. Sci.* 52 (2010) 179–186.
- [33] L.Q. Guo, M. Li, X.L. Shi, Y. Yan, X.Y. Li, L.J. Qiao, Effect of annealing temperature on the corrosion behavior of duplex stainless steel studied by in situ techniques, *Corros. Sci.* 53 (2011) 3733–3741.
- [34] J.A. Wharton, R.C. Barik, G. Kear, R.J.K. Wood, K.R. Stokes, F.C. Walsh, The corrosion of nickel–aluminium bronze in seawater, *Corros. Sci.* 47 (2005) 3336–3367.
- [35] G.W. Lorimer, F. Hasan, J. Iqbal, N. Ridley, Observation of microstructure and corrosion behavior of some aluminum bronzes, *Br. Corros. J.* 21 (1986) 244–248.